Published in final edited form as:
Cell. 2011 August 5; 146(3): 396–407. doi:10.1016/j.cell.2011.06.042.

MinD-dependent conformational changes in MinE required for the Min oscillator to spatially regulate cytokinesis

Kyung-Tae Park[1], **Wei Wu**[1], **Kevin P. Battaile**[2], **Scott Lovell**[3], **Todd Holyoak**[4], and **Joe Lutkenhaus**[1,*]

[1]Department of Microbiology, Molecular Genetics and Immunology, University of Kansas Medical Center, Kansas City KS 66160

[2]IMCA-CAT, Hauptman-Woodward Medical Research Institute, Sector 17, APS Argonne National Laboratory 9700 S. Cass Avenue, Bldg. 435A, Argonne, IL 60439 USA

[3]Structural Biology Center, University of Kansas, 2121 Simons Drive, Lawrence, KS 66047

[4]Department of Biochemistry and Molecular Biology, University of Kansas Medical Center, Kansas City KS 66160

Summary

MinD recruits MinE to the membrane leading to a coupled oscillation required for spatial regulation of the cytokinetic Z ring in *E. coli*. How these proteins interact, however, is not clear since the MinD binding regions of MinE are sequestered within a 6-stranded β-sheet and masked by N-terminal helices. Here, *minE* mutations are isolated that restore interaction to some MinD and MinE mutants. These mutations alter the MinE structure releasing the MinD binding regions and N-terminal helices that bind MinD and the membrane, respectively. Crystallization of MinD-MinE complexes reveals a 4-stranded β-sheet MinE dimer with the released β strands (MinD binding regions) converted to α-helices bound to MinD dimers. These results suggest a 6 stranded, β-sheet dimer of MinE 'senses' MinD and switches to a 4-stranded β-sheet dimer that binds MinD and contributes to membrane binding. Also, the results indicate how MinE persists at the MinD-membrane surface.

Introduction

Prokaryotes contain a family of proteins, designated the WACA family (Walker A cytomotive ATPase; also called ParA), that display oscillatory behavior involved in such diverse processes as spatial regulation of cell division, plasmid and chromosome segregation and regulation of development (Michie and Lowe, 2006). How this oscillatory behavior is achieved is not completely clear. The best studied member of the WACA family is MinD a component of the Min system involved in the spatial regulation of the positioning of the cytokinetic Z ring (Lutkenhaus, 2007).

In *E. coli* MinD and MinE undergo a rapid pole-to-pole oscillation that produces a time-averaged gradient of MinC, a passenger in the oscillation and an antagonist of FtsZ

*Corresponding author: Tel: (913) 588-7054, FAX: (913) 588-7295, jlutkenh@kumc.edu.

assembly, that is highest at the poles and lowest at midcell (de Boer *et al*., 1989; Fu *et al*., 2001; Hale *et al*., 2001; Hu and Lutkenhaus, 1999; Meinhardt and de Boer, 2001; Raskin and de Boer, 1999a). During the oscillation MinD, along with MinC, is present in a polar zone flanked near midcell by the MinE ring. Migration of the MinE ring towards the pole of the cell displaces MinD and MinC, which reassemble at the opposite pole, again flanked by a MinE ring near midcell.

Underlying the oscillation is the ATP-dependent interaction of the three Min proteins with each other and with the membrane (Lutkenhaus, 2007). MinD dimerizes in the presence of ATP and binds cooperatively to the membrane through a C-terminal amphipathic helix; dimerization is required for MinD to have sufficient affinity for the lipid bilayer (Hu and Lutkenhaus, 2003; Lackner et al., 2003; Szeto et al., 2003; Szeto et al., 2002; Wu *et al.* 2011). MinC and MinE are recruited to MinD and bind to overlapping sites located at the MinD dimer interface (Ma *et al*., 2004; Wu *et al*., 2011). MinC binding produces a potent inhibitor of Z ring assembly, whereas the binding of MinE, displaces MinC, stimulates the ATPase activity of MinD and triggers the release of MinD from the membrane (Hu *et al*., 2003; Lackner *et al*., 2003).

The apparent simplicity of the Min system has attracted modelers and experimentalists to determine the basis of dynamic pattern formation (Kruse *et al*., 2007). An important step was the demonstration that MinD and MinE are able to form travelling waves in vitro on a planar lipid bilayer in the presence of ATP that have characteristics of the in vivo oscillation. One study explained pattern formation by a reaction-diffusion mechanism (Loose *et al*., 2008) whereas another study emphasized surface-based mechanical stress arising from protein-membrane interactions involving multiple MinD-MinE species (Ivanov and Mizuuchi, 2010). More information is needed about the interaction between MinD and MinE to understand the structural basis of this self-organizing system.

MinE is a dimer of a small protein of 88 residues with two functional domains (Pichoff *et al*., 1995; Zhao *et al*., 1995). The N-terminal domain (residues ~6–31) is able to counteract MinCD's division inhibitory activity. Genetic studies suggest that this anti-MinCD domain forms an α-helix that binds MinD (Ma *et al*., 2003). The C-terminal domain (residues 32–88) is designated a topological specificity domain because it is required for MinE to spatially regulate cell division, presumably by dimerizing the anti-MinCD domains. Dimerization of these domains is essential as expression of $MinE^{22–88}$, which lacks part of the anti-MinCD domain, blocks cell division due to formation of heterodimers with WT MinE. These heterodimers are less efficient at countering MinCD (Zhang *et al*., 1998).

There are indications that MinE can interact directly with the membrane, although, recruitment of MinE to the membrane requires MinD (Raskin and de Boer, 1999a; Hu *et al*., 2002). For example, some MinE mutants, such as $MinE^{L22D}$ and $MinE^{I25R}$, bind directly to the membrane (Ma *et al*., 2003). The basis or significance of membrane binding by these mutants is not known. More recently, positively charged residues at positions 10–12 were implicated in MinE-membrane interaction (Hsieh *et al*., 2010). Also, in one of the models for Min oscillation formation of the MinE ring was achieved through MinE binding directly to the membrane after being recruited by MinD (Arjunan and Tomita, 2010).

The structures of two intact MinE proteins and one trypsin resistant fragment of MinE have been solved. Surprisingly, these structures differ significantly raising the possibility that they represent different conformational states. A trypsin resistant fragment of the *E. coli* MinE consists of residues 31–88 and is a dimer where each subunit consists of 2 anti-parallel β-strands packed against an α-helix (King *et al*., 2000). The helices pack together in the dimer to form an anti-parallel coiled coil and the βstrands (β2 & β3) form a 4-stranded, anti-

parallel β-sheet (Fig. 1A). The structures of the intact MinE's from *Helicobacter pylori* and *Neisseria gonorrhoeae* are also dimers, but contain a 6-stranded, anti-parallel β-sheet in addition to the α-helices (Kang et al., 2010). The additional β-strands (β1) containing part of the anti-MinCD domain are at the dimer interface sandwiched between the β-strands found in the structure of the truncated *E. coli* protein (Fig. 1B). In both of these structures the anti-MinCD domain is not solvent accessible and therefore unavailable for binding MinD. Additionally, in the *N. gonorrhoeae* structure a short N-terminal amphipathic helix (residues 3–8; residues 1–17 are not observed in the *H. pylori* structure) packs against the β-sheet further masking it (Fig. 1B). These structures suggest that the sequestered anti-MinCD domains (β1 strands) must be released to interact with MinD. Our study confirms this and reveals that both structures of the C-terminal domain of MinE (4 and 6-stranded) are physiologically relevant. We suggest that MinE senses MinD and undergoes a dramatic conformational change that releases the anti-MinCD domains and unmasks cryptic membrane targeting sequences (MTS) in MinE. These results lead to a model for MinD-MinE interaction that has implications for the mechanism of Min oscillation.

Results

Mutations altering MinE residue I24 restore interaction with some MinD mutants

Previously, we identified 13 MinD mutants that are defective in interaction with MinE but still activate MinC (Wu *et al*., 2011). To explore the MinD-MinE interaction we used the bacterial 2-hybrid system to select MinE mutants that regain interaction with these MinD mutants (Fig. 2A and Experimental Procedures). MinE mutants were isolated that regain interaction with 4 of these 13 MinD mutants. The amino acids altered in these 4 MinD mutants ($MinD^{M193L}$, $MinD^{D198R}$, $MinD^{G224C}$ and $MinD^{N222A}$) are located near each other at the MinD dimer interface close to the membrane (Fig. 1S). With $MinD^{M193L}$ we obtained $MinE^{I24N}$, which retained the ability to interact with WT MinD and also interacted with $MinD^{D198R}$ but not with the other MinD mutants (Fig. 2A, only 5 of the MinD mutants are shown). With $MinD^{D198R}$ we obtained $MinE^{I24S/E66G}$ and $MinE^{I24S/D45E}$ and with $MinD^{G224C}$ we obtained $MinE^{I24T/N16K}$ (data not shown). It was striking that in each of the MinE mutants, which retain the ability to interact with WT MinD, the I24 residue was altered.

The MinE mutants were tested in a physiological assay by assessing rescue of a Δ*min* strain from the expression of each of the 13 MinD mutants along with MinC. Only the MinD mutants (and WT MinD) that interact with the MinE mutants in the bacterial 2-hybrid system were rescued to some extent by the MinE mutants (Table S1). Further study revealed that the ability to rescue the MinD mutants is due to changes at position I24 as mutations that altered other residues (N16, D45 and E66) showed little ability to rescue on their own, even though they enhance rescue by mutations that alter I24 (Fig. 2B results with $MinD^{M193L}$; Table S1 for summary of results).

The isoleucine codon at position 24 is ATT and we obtained all three possible (due to a single nucleotide change) hydrophilic amino acid substitutions (Asn, Thr, Ser), but none of the possible hydrophobic amino acid substitutions (Val, Leu, Phe, Met). We hypothesized that the mutations altered the structure of MinE, which restored interaction with the MinD mutants. To test this further, we made multiple nucleotide changes to the ATT codon to yield arginine, glutamate, tryptophan, cysteine and valine. Consistent with our hypothesis, the hydrophilic substitutions along with the bulky tryptophan substitution resulted in a mutant MinE that was able to rescue $MinD^{M193L}$. Only $MinE^{I24V}$, containing a hydrophobic substitution, behaved like WT and was unable to rescue $MinD^{M193L}$ (Fig. 2C).

In the MinE structure from *N. gonorrhoeae* the residue corresponding to I24 is one of 3 large hydrophobic residues in the β1 strand that make hydrophobic interactions with the long α1 helix to generate a hydrophobic interior (Fig. 1B, residue in yellow). The I24 residue occupies the central position in the β1 strand and also makes hydrophobic interactions with itself so that a hydrophilic residue at position 24 would be very unfavorable. Although the I24 residue is also within the anti-MinCD domain, it is not required for binding MinD (Ma *et al*., 2003). One hypothesis to explain the I24 substitutions is that binding of MinE to MinD involves a 'sensing step' that leads to the release of the β1 strand (part of the anti-MinCD domain) so that it is available to bind MinD. In this scenario the four MinD mutants, such as $MinD^{M193L}$, are deficient in sensing MinE and inducing the release of the β1 strand. In MinE mutants, such as $MinE^{I24N}$, the β1 strand is already released so the 'sensing step' is bypassed. Another hypothesis is that two conformations of MinE exist in equilibrium and one is selected by MinD, however, we argue against this alternative based upon the failure of MinE to bind directly to the membrane (see discussion). To examine the first hypothesis we proceeded to determine if I24 substitutions altered the structure of MinE.

The *minE*^{I24N} mutation reduces the β strand content of MinE

To examine the effect of the *minE*^{I24N} mutation on the activity and structure of MinE we took advantage of the observation that ectopic expression of $MinE^{22–88}$ in a WT strain inhibits division and causes cell death due to $MinE^{22–88}$ forming a heterodimer with WT MinE (Pichoff *et al*., 1995; Zhang *et al*., 1998). In contrast, $MinE^{36–88}$ does not form a heterodimer with WT MinE nor inhibit division. Thus, filamentation offers a simple readout of the ability of N-terminally truncated MinEs to form heterodimers with WT MinE. Furthermore, since $MinE^{22–88}$ has most of the β1 strand intact for heterodimerization whereas $MinE^{36–88}$ is missing the β1 strand entirely these heterodimers are likely to be 6 β-stranded dimers (Fig. 1).

To test the 6-stranded heterodimer hypothesis we analyzed additional MinE constructs with an amino acid addition or deletion at the N-terminus of $MinE^{22–88}$. We suspected that these changes would enhance or hinder the ability of the resultant constructs to form heterodimers, respectively. Consistent with this, the inhibitory activity of $MinE^{21–88}$ was enhanced compared to $MinE^{22–88}$, whereas $MinE^{23–88}$ lacked inhibitory activity and behaved similarly to $MinE^{36–88}$ (Fig. 3A). Western blots demonstrated that the various MinEs derivatives had similar stability (data not shown).

We speculated above that the *minE*^{I24N} mutation caused release of the β1 strand from the dimer interface. If so, introducing the I24N substitution into $MinE^{21–88}$ should interfere with its ability to form heterodimers with WT MinE and inhibit division, and instead cause it to behave like $MinE^{23–88}$ and $MinE^{36–88}$. Consistent with this, $MinE^{21–88}$ with the I24N substitution ($MinE^{21–88(I24N)}$) did not inhibit division (Fig. 3A).

To examine the structural consequences of the *minE*^{I24N} mutation we analyzed the secondary structure content of $MinE^{21–88}$ and $MinE^{21–88(I24N)}$. The purified proteins were oligomers (Fig. S2A &B) and circular dichroism revealed they had similar α-helical content but that $MinE^{21–88(I24N)}$ had significantly reduced β-strand content and an increase in random coil (Fig. 3B and C). The calculated secondary structure content of $MinE^{21–88}$ from the circular dichroism data is consistent with the 6 β-stranded structure. For $MinE^{21–88(I24N)}$ the calculation is consistent with loss of the β1 strands from the dimer interface and their conversion to a random coil. Since $MinE^{21–88(I24N)}$ is a dimer (Fig. S2) we suggest that it is a 4 β-stranded dimer in which the β3 strands (Fig. 1A) come together to form the dimer interface as observed in the structure of the trypsin treated MinE (King *et al*., 2000). Based upon this reasoning and the inhibition data, MinE usually folds into the 6-stranded dimer but forms a 4-stranded dimer if formation of the 6-stranded dimer is compromised.

In contrast to the effect of the I24N substitution on the inhibitory activity of $MinE^{21–88}$, a different result is expected with the I25R substitution. We assume that the *minE*^{I25R} mutation affects MinE structure since $MinE^{I25R}$ binds directly to the membrane (Ma *et al*., 2003), although, it is unlikely to disrupt the MinE β-sheet structure. The I25 side chain, unlike the I24 side chain, is directed away from the large α1 helix (Fig. 1B, residue in green), and instead makes hydrophobic contacts with the N-terminal helix, which we designate a membrane targeting sequence (MTS, see below) (Ghasriani *et al*., 2010). Thus, the *minE*^{I25R} mutation is likely to disrupt this interaction and free the N-terminal helix without disrupting the 6 β-stranded structure. If so, it should not interfere with the ability of $MinE^{21–88}$ to form heterodimers and inhibit division. Consistent with this expectation, the I25R substitution had no effect on the ability of $MinE^{21–88}$ to cause filamentation and cell death when expressed in a WT strain (data not shown).

The N-terminal helix of MinE is a MTS responsible for promiscuous membrane binding of MinE mutants

Recruitment of WT MinE to the membrane requires MinD (Raskin and de Boer, 1999b; Hu *et al*. 2002), however, $MinE^{1–31}$ and several MinE mutants that do not bind MinD, including $MinE^{I25R}$ and $MinE^{L22R}$, bind directly to the membrane (Ma *et al*., 2003). This result raised the possibility that the N-terminal domain of MinE has a cryptic membrane targeting sequence (MTS) that is unmasked by mutation or possibly by interaction with MinD. Although membrane binding by $MinE^{1–31}$ has been attributed to positive charged residues located at positions 10–12, these residues do not appear to be masked in the most recent MinE structure (Hsieh *et al*., 2010; Ghasriani *et al*., 2010). Another possibility is that membrane binding is due to the short N-terminal amphipathic helix, which contains large conserved, hydrophobic residues that could function as a membrane targeting sequence (MTS) (Fig. 1B & S3). If so, mutations that release this amphipathic helix either by releasing the β1 strand (*minE*^{I24N} and *minE*^{L22R}) or interfering with its hydrophobic tethering (*minE*^{I25}) would produce constitutive membrane binding.

To test if this amphipathic helix is responsible for membrane binding in these mutants, we substituted a charged residue for each of the large hydrophobic residues and monitored their effects on membrane binding of $MinE^{I25R}$ tagged with GFP. Whereas $MinE^{I25R}$-GFP localized to the membrane, the introduction of any of 4 substitutions tested (L3E, L4E, F6E or F7E) abrogated membrane binding of $MinE^{I25R}$-GFP (Fig. 4A). Since we found that $MinE^{I24N}$ alters the structure of MinE we tested if it also led to membrane binding. Indeed, $MinE^{I24N}$-GFP was also targeted to the membrane independent of MinD (Fig. 4A). Introduction of any of the above charged substitutions also prevented $MinE^{I24N}$-GFP from going to the membrane (data not shown). These results demonstrate that the N-terminal amphipathic helix can function as an MTS.

Although the above results revealed that charged substitutions in the MTS of MinE blocked promiscuous membrane binding due to altering the structure of MinE, they did not reveal if this membrane binding was of physiological significance. To try and address this, the charged mutations were introduced into pSEB104CDE (P_{ara}::*minC minD minE*) and the resultant plasmids introduced into JS964 (*Δmin*) to determine if WT morphology was restored under inducing conditions. Surprisingly, the strains containing *minE*^{L3E} and *minE*^{F7E} were extremely filamentous and could not form colonies on plates with arabinose (Fig. 4B and data not shown) indicating MinE function was absent. In contrast, strains containing *minE*^{L4E} and *minE*^{F6E} formed colonies normally on plates with arabinose but the morphology of the cells were heterogeneous in length with some minicells. The average cell length of an exponential culture of the strain with *minE*^{WT} was 2.84 ± 0.89 μ compared to 4.68 ± 2.48 μ for the strain lacking Min function. The strains containing *minE*^{F6E} and *minE*^{L4E} had average cell lengths of 3.81 ± 2.67 μ and 2.95 ± 1.37μ, respectively (N~250 for

each). In summary, each of the 4 charge substitution mutations eliminated membrane binding of the MinE^{I25R} mutant. However, two of the mutations, *minE^{L3E}* and *minE^{F7E}*, completely eliminated the ability of MinE to counteract MinC/MinD, whereas the other two, *minE^{L4E}* and *minE^{F6E}*, did not, although they did reduce the ability of MinE to spatially regulate division as evidenced by the increases in the average cell length and the standard deviation.

The *minE^{I24N}* mutation also rescues some MinE mutants defective in interaction with MinD

The proposal that the anti-CD domain of MinE (~ residues 6–31) adopts an α helical conformation upon binding to MinD stemmed from a genetic study that revealed that residues important for binding MinD are located on one face of this putative helix (Ma *et al*., 2003). The exact length of this helix is uncertain but it does not appear to extend to position 8, which would be on the same face of the helix, since the L8R substitution did not affect binding to MinD (Ma *et al*., 2003). Although the L8R substitution was tested in the context of MinE$^{1–31}$, we confirmed that MinE^{L8R} was able to bind MinD (data not shown). In contrast, two of the MinE mutants we described above, MinE^{F7E} and MinE^{L3E}, were unable to rescue cells from expression of MinC/MinD (Fig. 4B). This was surprising since these residues lie beyond the putative interacting helix. We reasoned that these residues could play a role in 'sensing' MinD and therefore might have a defect in MinD-MinE interaction similar to the MinD^{M193L} mutant. If so, the *minE^{I24N}* mutation should suppress these mutations. As shown in Fig. 2D, the double mutant, MinE$^{F7E/I24N}$, rescued cells from expression of MinC/MinD demonstrating that the *minE^{I24N}* mutation is an intragenic suppressor of *minE^{F7E}*. It also suppressed *minE^{3LE}* (data not shown).

Although the *minE^{I24N}* mutation was able to suppress *minE^{F7E}* and *minE^{3LE}*, it should not suppress a MinE mutant that has a defect in the MinD binding surface. For example, the *minE^{I24N}* mutation was unable to suppress the *minE^{A18T}* mutation (Fig. 2D), which alters a residue near the middle of the putative helix thought to come into direct contact with MinD (Ghasriani *et al*., 2010; Ma *et al*., 2003). This result indicates A18 it is part of the binding surface.

Structure of the MinD-MinE^{I24N} complex

As one approach to explore the structural basis of the MinD-MinE interaction we purified MinE^{I24N} with a C-terminal His tag and tested interaction with MinD. It migrated slightly faster that WT MinE on SDS-PAGE and the MALDI spectrum revealed that MinE$^{I24N\text{-}h}$ was cleaved between amino acids 11 and 12 (designated MinE$^{I24N*\text{-}h}$). Several of the other MinE^{I24} mutants, MinE^{I24S} and the double mutant MinE$^{I24T/N16K}$, also underwent cleavage and, in all cases this occurred following cell lysis. The truncated MinE$^{I24N*\text{-}h}$ retained activity since it was able to stimulate ATP hydrolysis by MinD, although at ~50% of the activity of full length MinE (Fig. S4A).

We tested if MinE^{I24N}-h* could form a complex with MinD in the absence of phospholipid vesicles by assaying retention of MinD on a His-tag affinity column. MinDΔ10^{D40A} (a nonhydrolytic mutant that lacks its C-terminal amphipathic helix that also functions as a MTS) was retained on the column in the presence of MinE^{I24N}-h* in an ATP-dependent fashion (Fig. S4B). In fact, the retention of MinDΔ10^{D40A} on the column was greater in the presence of MinE^{I24N*}-h than with MinE-h. These results demonstrate that MinE^{I24N}-h* interacts with MinD even though it is missing the first 11 residues of MinE.

Our initial attempts to crystallize a MinD-MinE complex utilized MinDΔ10^{D40A} and WT MinE. However, adding ATP to a mixture containing these two proteins resulted in visible aggregation (perhaps due to release of the cryptic MTS of MinE). In contrast, aggregation

was not observed when ATP was added to a mixture of MinDΔ10^{D40A} and MinE^{I24N*}-h and crystals were obtained that diffracted to 4.3 Angstroms resolution (Table 1). The low resolution resulted from the high solvent content of the crystals (~70%) and attempts to improve resolution by dehydration or additive screening were not successful.

It was previously shown that a MinE$^{1–31}$ peptide binds MinD, but as we have shown here the first 11 residues of MinE are not essential. Therefore, we sought to obtain crystals of MinDΔ10^{D40A} with a synthetic peptide consisting of residues MinE$^{12–31}$. Crystals were obtained that diffracted to 2.6 Angstrom resolution (Table 1). The structure was solved by using MinDΔ10^{D40A} as a search model (Wu *et al*., 2011). Residues 13–26 of the MinE peptide, which includes most of the residues that correspond to the β1 strand of MinE, were visible in the structure as an α-helix, one present on each side of the MinD dimer interface (Fig. 5A and S5A; designated the contact helix). In the structure, the invariant R21 residue of MinE, required for stimulation of the MinD ATPase, forms hydrogen bonds with the side chain of E53 and backbone atoms of residues N222, S221 and L48 of MinD. Also, K19 forms a hydrogen bond with the side chain of D198. All 5 of these MinD residues are necessary for MinE binding (Wu *et al*., 2011). In addition, T14 of MinE forms a hydrogen bond with the side chain of residue N222. Since T14 had not previously been examined, we analyzed a *minET14A* mutation. It was unable to rescue a *Δmin* strain from expression of MinC/MinD indicating that T14 is important for the MinD-MinE interaction (data not shown). In addition, the I24 residue of MinE was on the side of the helix away from MinD as expected (Fig. 5A).

The structure of the MinDΔ10^{D40A}-MinE^{I24N}-h* complex was solved by molecular replacement using the structure of MinDΔ10^{D40A}-MinE$^{12–31}$ as a search model. The difference electron density map was consistent with an α–helix extending beyond residue residue 26 of MinE that was connected by a turn to a second helix (corresponding to α1 of MinE) that was near the midpoint of a second MinD dimer. Thus, it appeared that a MinE dimer was bridging two MinD dimers. A model of the trypsin resistant fragment of MinE (PDB:1EV0, residues 39–53) was superimposed on the difference density and the β-sheet regions were fit to the corresponding electron density and the model further refined (Fig. 5B and S5B; MinE is also shown in Fig. 1C). The asymmetric unit contains one MinD and one MinE dimer. In the crystal the dimers form a continuous helix along the 4_3 screw axis. Therefore, an alternate arrangement of the asymmetric unit could be represented as a single MinE dimer positioned between two MinD dimers that are related by the crystallographic symmetry operator (y+1/2, −x+1/2, z+1/4). In other words, a single MinE dimer is positioned between two MinD dimers related by the aforementioned symmetry operator (Fig. 5C).

Together the structures reveal several important features of the MinD-MinE interaction. The first is that the structure of MinE in the complex is consistent with a 4 stranded β-sheet but not with a 6 stranded β-sheet. Second, the β1 strand of MinE is present in an α helix (designated the ‘contact’ helix) that is at the MinD dimer interface, consistent with mutagenesis that identified MinD and MinE residues important for binding (Ghasriani *et al*., 2010; Hu and Lutkenhaus, 2001; Ma *et al*., 2004; Wu *et al*., 2011). Thus, the β1 strand (residues 21–29), containing part of the anti-MinCD domain, is stabilized as an α helix upon binding to MinD. Third, MinE bridges two MinD dimers leading to a continuous helix of alternating MinD dimers and MinE dimers. Since each MinD dimer is rotated 90° with respect to the previous one, only every fourth MinD dimer would be in contact with the membrane (Fig. 5B and S5C). It is not clear that the continuous helix is physiologically relevant (see discussion). Fourth, the N-terminus of the contact helix of MinE$^{I24N*-h}$ (residue 13) in the complex is oriented towards the membrane. As a result the MTS (not present in the crystal structure and indicated by dotted line in Fig. 5B) is on the same face of

the complex as the MinD amphipathic helices and therefore is in position to interact with the membrane.

Discussion

Based upon the results presented here and the available structures of free MinE a model emerges for the interaction between MinE and MinD. In this model MinE switches between a 'cryptic' cytoplasmic conformation that is freely diffusible and an 'active' conformation bound to MinD and the membrane. The active conformation is achieved by MinE sensing membrane bound MinD whereas conversion to the cryptic conformation occurs following stimulation of the MinD ATPase and release from the membrane. Essential to this model is the dual role of residues ~21–29 of MinE; as the β1 strand sequestered at the MinE dimer interface and as the contact helix involved in binding MinD (Fig. 1B–D).

In the model MinE senses a MinD dimer at the membrane and undergoes a conformational change that releases the MTSs and the β1 strands with the C-terminal domain collapsing to a 4 stranded β-sheet (Fig. 5B and 1C). The β1-strand near MinD, along with additional N-terminal residues (~12–20), is stabilized as an α helix (the contact helix) upon binding MinD. Importantly, the orientation of the contact helix bound to MinD positions the MTS of MinE near the membrane (Fig. 5B). The released β1 strand not immediately in contact with a MinD dimer is tethered to the membrane by a contiguous MTS (Fig. 6). Following stimulation of the MinD ATPase, MinD is released from the membrane and MinE either 'snaps back' to the 6-stranded β-sheet structure and dissociates from the membrane or is handed off to another MinD dimer (Fig. 6 and discussion below).

Residue I24 occupies a unique position in MinE since it can be altered to release the β1 strand but is not required for MinD binding. The I24N substitution reduced the β strand content of $MinE^{21–88}$ and we propose that this substitution in full-length MinE releases the β1 strand so that it is available for interaction with MinD. This effect of the $minE^{I24N}$ mutation to 'open up' the MinE structure allows it to suppress some of the mutations in *minD* (*M193L, D198R, N22A and G224C*) and *minE* (*L3E and F7E*) that prevent interaction. Thus, the residues of MinD and MinE identified by these mutations are likely involved in the 'sensing step' that triggers the conversion of MinE from the 6 to the 4 β-stranded structure. On the other hand, mutations not suppressed by the $minE^{I24N}$ mutation, such as $minE^{A18T}$ and $minD^{E53K}$, likely identify residues directly involved in binding. This latter possibility is confirmed by the structure of the complex.

MinE residues important for stimulating the MinD ATPase (and also for binding) include R21, L22 and A18. Residue R21 forms a hydrogen bond with E53 of MinD and the backbone of residues N222, S221 and L48, all of which were recently shown to be important for MinE binding (Wu *et al*., 2011). In addition, residues L22 and A18 abut MinD whereas residues I24 and E20, which are not important for binding, are on the face of the contact helix away from MinD (Fig. 5A). Although MinE stimulates the MinD ATPase, the mechanism is not clear. One possibility suggested for another WACA family member (ParF) - that a conserved arginine in its partner (ParG) functions as an arginine finger (Barilla *et al*., 2007) – can be ruled out. The conserved arginine, R21, in MinE interacts with MinD residue E53 and is not near the catalytic site (Fig. 5B). MinE likely stimulates the ATPase of MinD by inducing subtle changes in the switch regions of MinD similar to what is observed in the nitrogenase complex (Schindelin *et al*., 1997).

One possible mechanism for the MinD-dependent conversion of MinE from the 6 to the 4 β-stranded structure is that the two structures are in equilibrium and that MinD binding to the 4 stranded structure pulls the equilibrium in this direction. However, we think this is

unlikely since the 4-stranded structure (such as $MinE^{I24N}$) binds to the membrane independent of MinD. If the two structures were in equilibrium in WT MinE, one would expect WT MinE to go to the membrane independent of MinD (the binding to the membrane by the 4 stranded structure would pull the equilibrium in that direction).

Although the MTS contains highly conserved hydrophobic residues (Fig. S3), no function has been ascribed to this segment of MinE. Our study indicates it is a cryptic MTS that can be umasked by mutation or through interaction with MinD. A previous study argued that positively charged residues were involved in direct MinE-membrane interaction since eliminating 3 charged residues (C1 mutant - positions 10–12) affected the interaction of $MinE^{1–31}$ with vesicles *in vitro* and Min oscillation *in vivo* (Hsieh *et al*., 2010). Although these residues could also contribute to membrane binding, they are also involved in 'sensing' MinD as altering these residues also affects the ability of MinE to displace MinC from MinD (Loose *et al*., 2011).

In WT MinE the MTS is packed against the β-sheet and not available for interaction with the membrane (Fig. 1B). Therefore, it is not surprising that mutations that disrupt the 6-stranded β-sheet structure, such as $minE^{I24N}$ and $minE^{L22R}$, release this MTS so that it is available to interact with the membrane. These mutations mimic the interaction with MinD to open up the MinE structure. In contrast, the $minE^{I25R}$ mutation induces membrane binding, not by disrupting the β-sheet structure, but by disrupting the hydrophobic interaction that tethers the MTS to the β-sheet (Fig. 1B).

Although all 4 of the *minE* charge mutations ($minE^{L3E}$, $minE^{L4E}$, $minE^{F6E}$ and $minE^{F7E}$) prevented MinE mutants (I25R and I24N) from going to the membrane, their effect on the ability of MinE to counter MinC/MinD varies. One possible explanation for this difference is the position of the corresponding amino acids in the MTS. Residues L3 and F7 interact with residue I25 to tether the MTS to the β-sheet whereas L4 and F6 do not (Fig. 1B; Ghasriani *et al*., 2010). Thus, substituting a charged residue for L3 or F7 would release the MTS and the loop formed by residues 8–20 would no longer be constrained, which is likely to be important for sensing.

Residues L3 and F7 could be the most important of the hydrophobic residues for membrane binding but their additional involvement in sensing MinD makes this difficult to determine. Nonetheless, a role for the interaction of MinE with the membrane is indicated by the effect of the $minE^{F6E}$ and $minE^{L4E}$ mutations on cell morphology. Even though these mutations do not significantly affect MinD binding, strains with these mutations have a heterogeneous size distribution indicating that membrane binding by MinE contributes to spatial regulation. This is consistent with the phenotype previously observed with $MinE^{6–88}$, which suppresses the inhibitory activity of MinD/MinC but produces a phenotype resembling what we observe with $minE^{F6E}$ and $minE^{L4E}$ (Pichoff *et al*., 1995).

Importance of the MinE dimer – Tarzan of the jungle

Previous work indicated that the dimerization of MinE is important for its anti-MinC/MinD activity (Pichoff *et al*., 1995; Zhao *et al*., 1995). The basis for this conclusion is the observation that heterodimers formed between WT MinE and $MinE^{22–88}$ have reduced activity (Zhang *et al*., 1998). Formation of these heterodimers does not alter the total concentration of anti-MinCD domains in the cell, but simply limits each MinE dimer to one anti-MinCD domain. This monomerization of the anti-MinCD domains is sufficient to reduce their activity so at physiological levels they no longer counteract MinC/MinD and cells fail to divide.

The MinE C-terminal domain is necessary for spatial regulation of division. It has three known functions: sequestering and dimerizing the anti-MinCD domains and restraining the MTS so it does not interact with the membrane. As proposed here, MinE encountering a MinD dimer at the membrane releases the MTSs and the β1 strands, one of which becomes the contact α helix and binds to the encountered MinD dimer with the immediately adjacent MTS interacting with the membrane. The other released anti-MinCD domain is probably a nascent helix tethered to the membrane through its linked MTS (Fig. 6).

It is possible that a MinE dimer bridges two membrane bound MinD dimers as observed in the crystal, however, the two MinD dimers are rotated 90° with respect to each other due to the angle of the MinE arms (Fig. S4B). If the junction between the contact helix and α1 is flexible, this is possible. We favor a “Tarzan traveling on vines through the jungle” model, with MinE as Tarzan and MinD as the vine (Fig. 6). Like Tarzan, MinE has two arms and swings from MinD (the vine) to MinD. In the model MinE bound to MinD has two alternatives following stimulation of the MinD ATPase and its release from the membrane. MinE, either dissociates from the membrane as it reverts back to the cryptic form, or before this happens, an anti-MinCD domain grasps a second MinD dimer. It is possible that MinE has an intermediate, transient membrane associated state free of MinD. In the Tarzan analogy, once he grabs the vine it has a finite lifetime before it falls from the trees and he has to grab another vine or he suffers the same fate and has to start over. A high, local density of MinD on the membrane favors a successful ‘handoff’ whereas a lower density favors MinE ‘snapping’ back to the 6 stranded structure and being released from the membrane. The rates of these two competing reactions dictate the fate of the MinE (Fig. 6, a&b).

A recent report examining the Min system *in vitro* (Loose *et al*., 2011) found that the residence time for MinE in a traveling wave was longer than for MinD. It is likely that the ability of MinE to ‘swing from one MinD to the next’ explains the longer MinE residence times. It is also clear in this model why MinE tracks membrane bound MinD and moves towards regions of higher MinD density. Finally, our findings here about the MinD-MinE system are likely to be applicable to other members of the WACA family.

Experimental Procedures

A detailed methods description can be found in the Extended Experimental Procedures section.

Bacterial strains and growth conditions

E. coli strains JS964 (MC1061 *malP::lacI*^{q} *Δmin::kan*) and its isogenic parental strain JS219 (*minCDE*$^{+}$) have previously been described (Pichoff *et al*., 1995). LB (Luria-Bertani) medium containing 0.5% NaCl and relevant antibiotics at 37°C was used for most experiments unless otherwise indicated. BTH101Δ*min* (F^{-} *cya*-99, *ara*D139, *gal*E15, *gal*K16, *rps*L1 (Str^{r}), *hsd*R2, *mcr*A1, *mcr*B1 Δ*min::kan*) was used for bacterial 2-hybrid system (Wu *et al*., 2011).

Plasmids

Most of the plasmids have been previously described and are detailed in the Extended Experimental Procedures. Plasmids new to this study expressed MinE in which part of the N-terminus was replaced with a his-tag and were constructed as follows. *minE* fragments were obtained by PCR using pSEB104CDE as a template and were ligated into EcoRI/XbaI-treated pQE80L (Qiagen) to generate pQE80L-MinE$^{21–88}$, pQE80L-MinE$^{22–88}$, pQE80L-

MinE$^{23–88}$, and pQE80L MinE$^{36–88}$. A derivative of pQE80L-MinE$^{21–88}$ carrying the I24N substitution was made by site-directed mutagenesis.

Bacterial two-hybrid analysis

A *cya*-null strain BTH101*Δmin::kan* was transformed with plasmids pCT25-MinD and pUT18-MinE, respectively carrying wild-type or mutant *minD* and *minE* alleles, and grown overnight at 37°C on LB plates containing 0.2% glucose, 20 μg/ml chloramphenicol and 100 μg/ml ampicilin. For a plate-based assay, colonies from the LB plate were diluted in 300 μl volume of LB broth and spotted onto fresh LB plates supplemented with 20 μg/ml chloramphenicol, 100 μg/ml ampicilin, 40 μg/ml 5-bromo-4-chloro-3-indoyl-β-D-galactopyranoside (X-Gal), and 0.5 mM IPTG. Observation was usually made after 14–18 hours of incubation at 30°C.

Random mutagenesis of MinE

Mutations were introduced into *minE* using the GeneMorph II Random Mutagenesis kit (Stratagene) as described in the Expanded Experimental Procedures.

Overexpression and purification of MinD and MinE proteins

MinDΔ10^{D40A} and C-terminal or N-terminal his-tagged versions of derivatives of MinE were purified using expression plasmids as described in the Expanded Experimental Procedures.

Gel filtration and circular dichroism (CD) Spectroscopy

Protein samples (500 μl volume) at a final concentration of 1 μg/ml were diluted in buffer C (25 mM HEPES-NaOH [pH7.0], 250 mM NaCl, 1 mM EDTA, 5 mM DTT) before being subjected to an AKA-fast protein liquid chromatography equipped with Superdex^{TM}75HR 10/30 column (GE Healthcare) with a flow rate of 0.5 ml/min. For CD analysis, MinE$^{21–88}$ and MinE$^{21–88\text{-}I24N}$ samples at a concentration of 570 μM were prepared by 100-fold dilution in 10 mM sodium phosphate buffer (pH 7.5). Far-UV CD spectra were recorded on a Jasco - spectropolarimete C. Spectra were an average of 10 scans over the wavelength from 190 nm to 250 nm. The secondary structure content of each sample was obtained using the K2d prediction program (Andrade *et al*., 1993).

Microscopy

Strain JS964 (Δ*min*)/pSEB104CDE and JS964(Δ*min*)/pSEB104CDE-24 were grown overnight at 37°C in LB medium containing 0.1% arabinose and 100 μg/ml spectinomycin. The next day, cells were diluted and cultured under the same conditions described above to an OD_{560} of 0.4–0.5. The phenotypes of cells were characterized using a Nikon microscope equipped with a 100 X objective. To determine subcellular localization of MinE proteins, cultures of JS964 (Δ*min*)/pJK110P_{lac}*::minE^{I24N}*-GFP, JS964(Δ*min*)/pJK100 (P_{lac}::*minD minE-GFP*), and JS964(Δ*min*)/pDSW208 (P_{lac}*::minD minE^{I24N}-GFP*) in exponential phase were incubated with 10 μM IPTG for 1 hour at 37°C in LB. The images were recorded at 15 second intervals using a cooled CCD camera and processed using Metamorph and Adobe Photoshop.

Crystallization and Structure determination

The growth of crystals and the determination of the structures by X-ray crystallography are described in full in the Extended Experimental Procedures. In brief, crystals of MinDΔ10^{D40A} and MinE^{I24}-h* diffracted to 4.3 Å resolution and crystals of MinDΔ10^{D40A} and a synthetic peptide of MinE$^{12–31}$ diffracted to 2.6 Å resolution. The accession codes are 3R9I for MinD-MinE$^{12–31}$ and 3R9J for MinD-MinE$^{I24N*\text{-}h}$.

Supplementary Material

Refer to Web version on PubMed Central for supplementary material.

Acknowledgments

This work was supported by grant GM29764 from the National Institutes of Health to JL. We thank members of the lab for discussion and Alex Dajkovic for reading of the manuscript. Use of the IMCA-CAT beamline 17-ID at the Advanced Photon Source was supported by the companies of the Industrial Macromolecular Crystallography Association through a contract with Hauptman-Woodward Medical Research Institute. Use of the Advanced Photon Source was supported by the U.S. Department of Energy, Office of Science, Office of Basic Energy Sciences, under Contract No. DE-AC02-06CH11357. Use of the KU COBRE Protein Structure Laboratory was supported by NIH Grant Number P20 RR-17708 from the National Center for Research Resources.

References

Andrade MA, Chacon P, Merelo JJ, Moran F. Evaluation of secondary structure of proteins from UV circular dichroism spectra using an unsupervised learning neural network. Protein Eng. 1993; 6:383–390. [PubMed: 8332596]

Arjunan SN, Tomita S. A new multicompartmental reaction-diffusion modeling method links transient membrane attachment of *E. coli* MinE to E-ring formation. Syst Synth Biol. 2010; 4:35–53. [PubMed: 20012222]

Barilla D, Carmelo E, Hayes F. The tail of the ParG DNA segregation protein remodels ParF polymers and enhances ATP hydrolysis via an arginine finger-like motif. Proc Natl Acad Sci U S A. 2007; 104:1811–1816. [PubMed: 17261809]

de Boer PA, Crossley RE, Rothfield LI. A division inhibitor and a topological specificity factor coded for by the minicell locus determine proper placement of the division septum in *E. coli*. Cell. 1989; 56:641–649. [PubMed: 2645057]

Evans P. Scaling and assessment of data quality. Acta Crystallogr D Biol Crystallogr. 2006; 62:72–82. [PubMed: 16369096]

Fu X, Shih YL, Zhang Y, Rothfield LI. The MinE ring required for proper placement of the division site is a mobile structure that changes its cellular location during the *Escherichia coli* division cycle. Proc Natl Acad Sci U S A. 2001; 98:980–985. [PubMed: 11158581]

Ghasriani H, Ducat T, Hart CT, Hafizi F, Chang N, Al-Baldawi A, Ayed SH, Lundstrom P, Dillon JA, Goto NK. Appropriation of the MinD protein-interaction motif by the dimeric interface of the bacterial cell division regulator MinE. Proc Natl Acad Sci U S A. 2010; 107:18416–18421. [PubMed: 20937912]

Hale CA, Meinhardt H, de Boer PA. Dynamic localization cycle of the cell division regulator MinE in *Escherichia coli*. EMBO J. 2001; 20:1563–1572. [PubMed: 11285221]

Hsieh CW, Lin TY, Lai HM, Lin CC, Hsieh TS, Shih YL. Direct MinE-membrane interaction contributes to the proper localization of MinDE in *E. coli*. Mol Microbiol. 2010; 75:499–512. [PubMed: 20025670]

Hu Z, Lutkenhaus J. Topological regulation of cell division in *Escherichia coli* involves rapid pole to pole oscillation of the division inhibitor MinC under the control of MinD and MinE. Mol Microbiol. 1999; 34:82–90. [PubMed: 10540287]

Hu Z, Lutkenhaus J. Topological regulation of cell division in *E. coli*. spatiotemporal oscillation of MinD requires stimulation of its ATPase by MinE and phospholipid. Mol Cell. 2001; 7:1337–1343. [PubMed: 11430835]

Hu Z, Lutkenhaus J. A conserved sequence at the C-terminus of MinD is required for binding to the membrane and targeting MinC to the septum. Mol Microbiol. 2003; 47:345–355. [PubMed: 12519187]

Hu Z, Gogol EP, Lutkenhaus J. Dynamic assembly of MinD on phospholipid vesicles regulated by ATP and MinE. Proc Natl Acad Sci U S A. 2002; 99:6761–6768. [PubMed: 11983867]

Hu Z, Saez C, Lutkenhaus J. Recruitment of MinC, an inhibitor of Z-ring formation, to the membrane in *Escherichia coli*: role of MinD and MinE. J Bacteriol. 2003; 185:196–203. [PubMed: 12486056]

Ivanov V, Mizuuchi K. Multiple modes of interconverting dynamic pattern formation by bacterial cell division proteins. Proc Natl Acad Sci U S A. 2010; 107:8071–8078. [PubMed: 20212106]

Kang GB, Song HE, Kim MK, Youn HS, Lee JG, An JY, Chun JS, Jeon H, Eom SH. Crystal structure of *Helicobacter pylori* MinE, a cell division topological specificity factor. Mol Microbiol. 2010; 76:1222–1231. [PubMed: 20398219]

King GF, Shih YL, Maciejewski MW, Bains NP, Pan B, Rowland SL, Mullen GP, Rothfield LI. Structural basis for the topological specificity function of MinE. Nat Struct Biol. 2000; 7:1013–1017. [PubMed: 11062554]

Kruse K, Howard M, Margolin W. An experimentalist's guide to computational modelling of the Min system. Mol Microbiol. 2007; 63:1279–1284. [PubMed: 17302810]

Lackner LL, Raskin DM, de Boer PA. ATP-dependent interactions between *Escherichia coli* Min proteins and the phospholipid membrane in vitro. J Bacteriol. 2003; 185:735–749. [PubMed: 12533449]

Loose M, Fischer-Friedrich E, Ries J, Kruse K, Schwille P. Spatial regulators for bacterial cell division self-organize into surface waves in vitro. Science. 2008; 320:789–792. [PubMed: 18467587]

Loose M, Fischer-Friedrich E, Harold C, Kruse K, Schwille P. Single-molecule imaging of Min protein dynamics reveals the general propoerties of pattern formation. Nat Struct Mol Biol. 2010; 18:577–83. [PubMed: 21516096]

Lutkenhaus J. Assembly dynamics of the bacterial MinCDE system and spatial regulation of the Z ring. Annu Rev Biochem. 2007; 76:539–562. [PubMed: 17328675]

Ma L, King GF, Rothfield L. Positioning of the MinE binding site on the MinD surface suggests a plausible mechanism for activation of the *Escherichia coli* MinD ATPase during division site selection. Mol Microbiol. 2004; 54:99–108. [PubMed: 15458408]

Ma LY, King G, Rothfield L. Mapping the MinE site involved in interaction with the MinD division site selection protein of *Escherichia coli*. J Bacteriol. 2003; 185:4948–4955. [PubMed: 12897015]

Meinhardt H, de Boer PA. Pattern formation in *Escherichia coli*: a model for the pole-to-pole oscillations of Min proteins and the localization of the division site. Proc Natl Acad Sci U S A. 2001; 98:14202–14207. [PubMed: 11734639]

Michie KA, Lowe J. Dynamic filaments of the bacterial cytoskeleton. Annu Rev Biochem. 2006; 75:467–492. [PubMed: 16756499]

Pichoff S, Vollrath B, Touriol C, Bouche JP. Deletion analysis of gene *minE* which encodes the topological specificity factor of cell division in *Escherichia coli*. Mol Microbiol. 1995; 18:321–329. [PubMed: 8709851]

Raskin DM, de Boer PA. MinDE-dependent pole-to-pole o scillation of division inhibitor MinC in *Escherichia coli*. J Bacteriol. 1999a; 181:6419–6424. [PubMed: 10515933]

Raskin DM, de Boer PA. Rapid pole-to-pole oscillation of a protein required for directing division to the middle of *Escherichia coli*. Proc Natl Acad Sci U S A. 1999b; 96:4971–4976. [PubMed: 10220403]

Schindelin H, Kisker C, Schlessman JL, Howard JB, Rees DC. Structure of ADP-AlF4--stabilized nitrogenase complex and its implications for signal transduction. Nat. 1997; 387:370–377.

Szeto TH, Rowland SL, Habrukowich CL, King GF. The MinD membrane targeting sequence is a transplantable lipid-binding helix. J Biol Chem. 2003; 278:40050–40056. [PubMed: 12882967]

Szeto TH, Rowland SL, Rothfield LI, King GF. Membrane localization of MinD is mediated by a C-terminal motif that is conserved across eubacteria, archaea, and chloroplasts. Proc Natl Acad Sci U S A. 2002; 99:15693–15698. [PubMed: 12424340]

Weiss MS. Global indicators of X-ray data quality. Journal of Applied Crystallography. 2001; 34:130–135.

Wu W, Park KT, Holyoak T, Lutkenhaus J. Determination of the structure of the MinD-ATP complex reveals the orientation of MinD on the membrane and the relative location of the binding sites for MinE and MinC. Mol Microbiol. 2011; 79:1515–1528. [PubMed: 21231967]

Zhang Y, Rowland S, King G, Braswell E, Rothfield L. The relationship between hetero-oligomer formation and function of the topological specificity domain of the *Escherichia coli* MinE protein. Mol Microbiol. 1998; 30:265–273. [PubMed: 9791172]

Zhao CR, de Boer PA, Rothfield LI. Proper placement of the *Escherichia coli* division site requires two functions that are associated with different domains of the MinE protein. Proc Natl Acad Sci U S A. 1995; 92:4313–4317. [PubMed: 7753804]

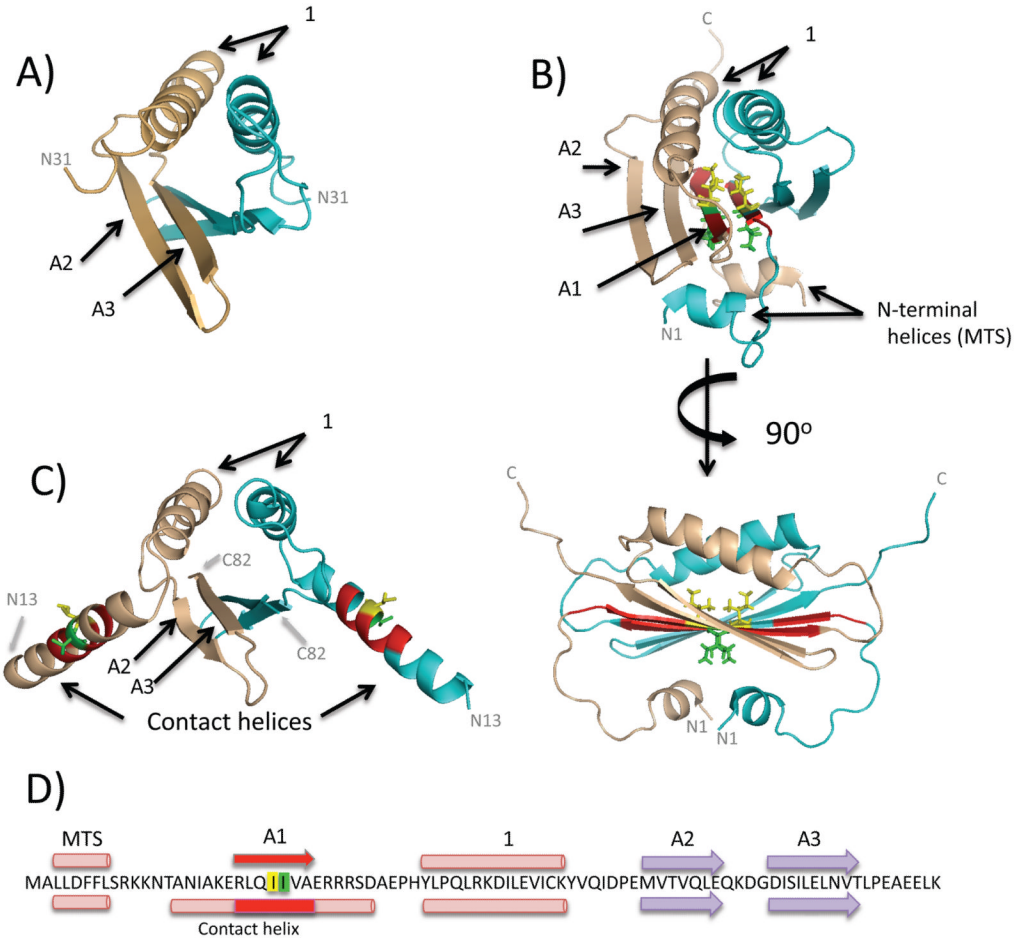

Fig. 1.

Structures of MinE and location of critical residues. The structure of the trypsin-treated MinE (residues 31–88) from *E. coli* (A) and two views of the the MinE (residues 1–89) from *N. gonnorrhoeae* (B) are shown (PDBs 1EVO and 2KXO, respectively). These structures contain 4-stranded and 6-stranded β-sheets, respectively. The labeling of secondary structural elements follows the labeling of the *N. gonnorrhoeae* structure. The N-terminal helices are shown in this study to function as a membrane targeting sequence (MTS). The residue corresponding to I24 of the *E. coli* MinE is colored yellow in this structure and the residue corresponding to I25 is colored green. (C) The structure of $MinE^{12–88(I24N)}$ from the MinD-MinE complex reported in this work (residues 13–83 of MinE are visible). Note that it is a 4-stranded β-sheet and the region corresponding to β1 in panel B (red) is part of an α helix (the contact helix). The N- and C-termini are indicated. (D) The sequence of MinE from *E. coli* with the secondary structural elements present in free MinE displayed above the sequence and those present in MinE in the complex with MinD displayed below the sequence.

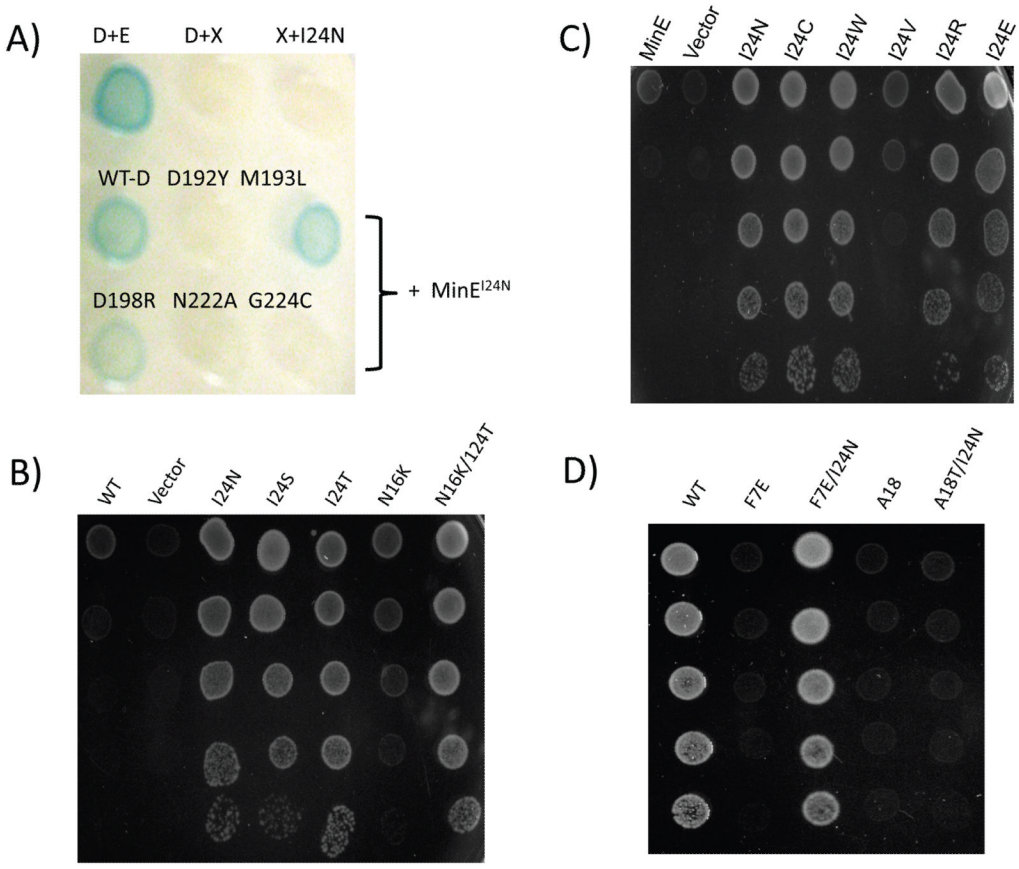

Fig. 2.

Analysis of the ability of MinE mutants to bind to MinD mutants and suppress MinC/MinD inhibitory activity. A) Bacterial two-hybrid analysis of the interaction between $MinE^{I24N}$ and several MinD mutants. First row (controls): MinD + MinE, MinD + X and X + $MinE^{I24N}$ (X=empty vector); the second and third row contain $MinE^{I24N}$ in combination with the indicated MinD mutant. B) The ability of various *minE* alleles to suppress killing by MinC/$MinD^{M193L}$. JS964 (*Δmin*)/pSEB104CD-193 (P_{ara}::*minC minD*^{M193L}) with pJB216 (P_{lac}::*minE*) derivatives containing the indicated *minE* allele were serially diluted 10 fold and spotted on plates containing 0.1% arabinose and 100 μM IPTG. C) As in panel B. D) The *minE*^{I24N} mutation suppresses some, but not all, *minE* mutations. pJB216 (P_{lac}::*minE*) derivatives carrying the *minE* alleles indicated were tested for their ability to protect JS964 (*Δmin*) from the induction of MinC/MinD from pSEB104CD (P_{ara}::*minC minD*).

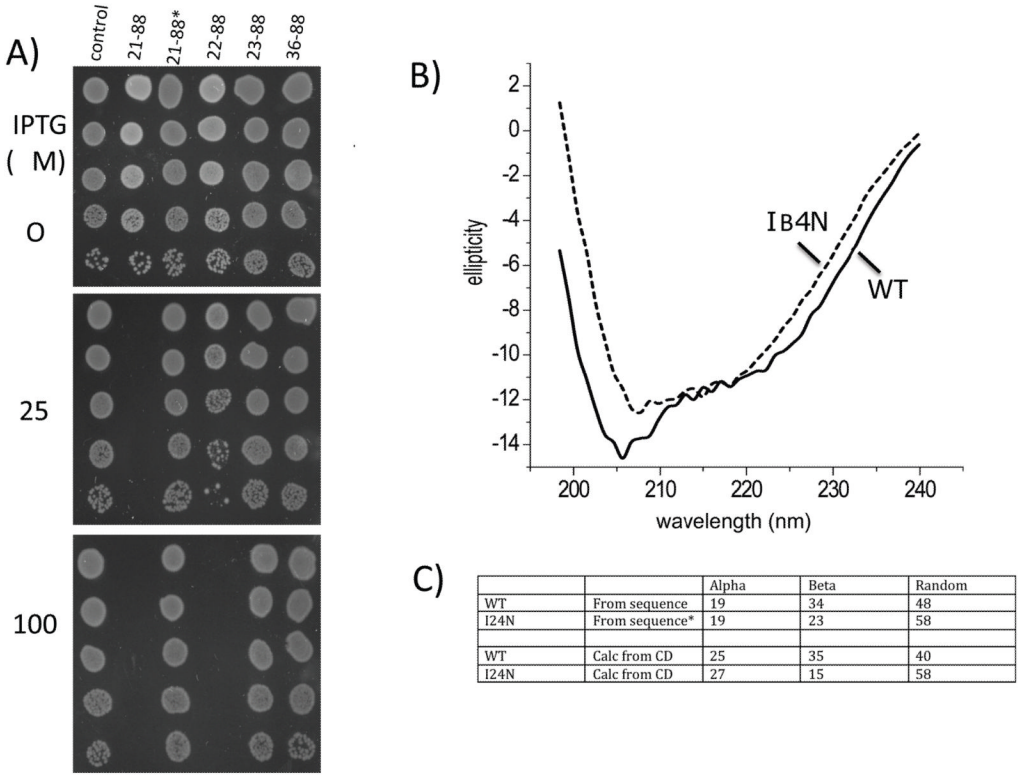

		Alpha	Beta	Random
WT	From sequence	19	34	48
I24N	From sequence*	19	23	58
WT	Calc from CD	25	35	40
I24N	Calc from CD	27	15	58

Fig. 3.

Inhibitory activity and secondary structure of N-terminal truncated MinEs. A) The sensitivity of JS219 (*min*$^+$) to N-terminally truncated MinEs was determined by spotting serial (10-fold) dilutions of cultures of JS219 containing plasmids expressing various N-terminal truncated MinE derivatives on plates containing IPTG as indicated. The control is the parent vector without an insert. The presence of the I24N substitution is indicated by the asterisk. B) Circular dichroism spectra of MinE$^{21–88}$ and MinE$^{21–88(I24N)}$. C) The % of secondary structure content was estimated from the CD spectra using the K2d prediction program (Andrade *et al*., 1993) and is compared to the % of secondary structure content present in the crystal structure of MinE (corresponding to residues 21–88) from *H. pylori*. The asterisk indicates that the value for β content of MinE$^{21–88(I24N)}$ was calculated assuming the β1 strand is a random coil.

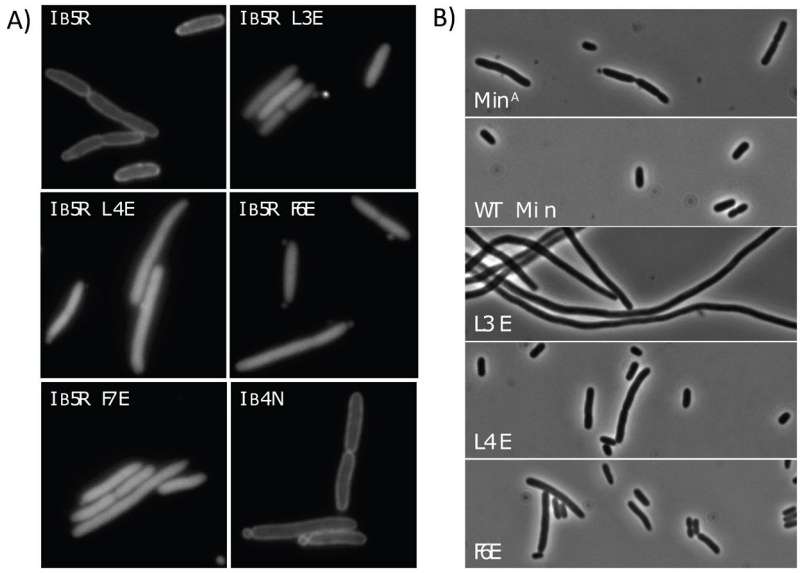

Fig. 4.

Effect of *minE* mutations on membrane localization of MinE and its ability to counter MinC/MinD. A) JS964 (Δ*min*) containing pJK100 (P_{trc}*::minE-gfp*) derivatives expressing *minE-GFP* fusions with the indicated *minE* mutations were analyzed by fluorescence microscopy. The strains were grown in the presence of 20 μM IPTG. B) The effect of *minE* mutations on spatial regulation of cell division. JS964 (Δ*min*) containing pSEB104CDE (P_{ara}*::minC minD minE*) derivatives containing various *minE* mutations (as indicated in the panels) was grown to exponential phase with 0.1% arabinose for 24 hours to induce the *min* operon. The first panel contained the $minC^{R133A}$ mutation, which prevents interaction with MinD and inactivates Min function (Zhou and Lutkenhaus, 2005).

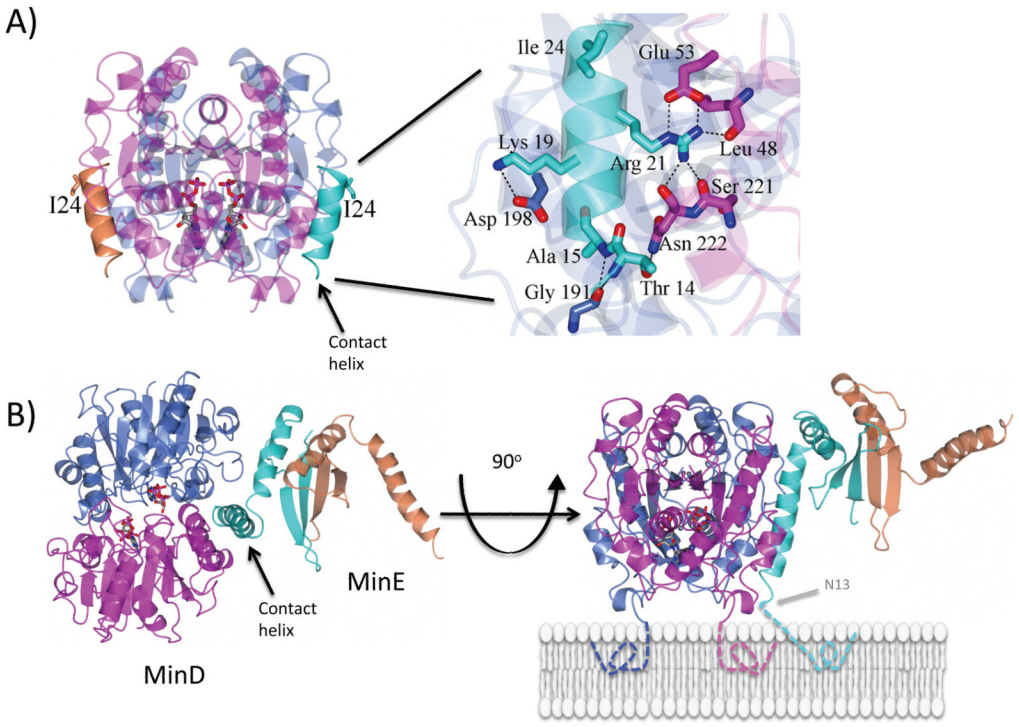

Fig. 5.

Structure of the MinE-MinD complex. Panel (A) contains the complex between MinDΔ10^{D40A} and MinE$^{12–31}$ (only residues 13–26 are visible). The structure shows a MinE peptide (contact helix; colored cyan and organe) bound to each side of a MinD dimer (magenta and blue: ADP in red). On the right is a blowup of the MinE contact helix bound to MinD. It is rotated 90°. Hydrogen bonds are indicated by dashed lines. The I24 residue is on the side of the helix away from MinD. Panel (B) shows the structure of the complex between MinDΔ10^{D40A} and MinE^{I24N}*-h (both dimers). In the crystal the dimers alternate to make a continuous helix (Fig. S5C). In the orientation on the left the membrane binding surface of MinD is beneath MinD so that the N-terminus of the contact helix (residue 13) is directed into the plane of the figure. In the structure on the right the MinD-MinE complex is rotated 90° so the orientation with respect to the membrane can be observed. The MTSs of MinD and MinE are depicted with dotted lines.

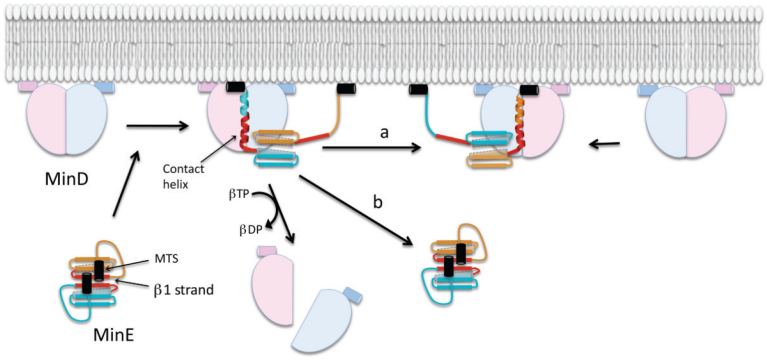

Fig. 6.

Tarzan of the Jungle model for the interaction between MinD and MinE. In this model MinE encounters MinD bound to the membrane and the MTSs (black segments) and the β1 strands (red) of MinE are released from the 6 stranded β-sheet structure resulting in formation of a 4-stranded β-sheet structure. One of the released β1 strands along with N-terminal flanking residues form an α-helix that is stabilized by binding to MinD while the other is tethered to the membrane through its linked MTS. The fate of MinE depends on two competing reactions (indicated by ‘a’ and ‘b’) following the dissociation of MinD due to ATPase stimulation. Either it is handed off to another MinD (a) or dissociates from the membrane as it snaps back to the 6 β-stranded structure (b). A higher density of MinD on the membrane favors the former.

Table 1

Crystallographic data for MinD-MinE structures

	MinD-MinE [12–31]	MinD-MinE^{I24N}*-h
Data Collection		
Unit-cell parameters (Å, °)	a=64.29, b=71.80, c=76.64 α=102.64, β=95.87, γ=111.72	a=94.39, c=284.98 α=β=γ=90
Space group	$P1$	$P4_32_12$
Resolution (Å)[1]	73.24-2.60 (2.74-2.60)	50.0-4.30 (4.53-4.30)
Wavelength (Å)	1.0000	1.0000
Temperature (K)	100	100
Observed reflections	129,007	121,143
Unique reflections	36,883	9,437
Mean <I/σI>[1]	7.1 (2.4)	15.4 (5.5)
Completeness (%)[1]	98.5 (98.2)	99.9 (100)
Multiplicity[1]	3.5 (3.5)	12.8 (12.4)
R_{merge} (%)[1, 2]	15.3 (56.6)	10.8 (52.3)
R_{meas}[4]	18.2 (67.4)	11.3 (54.5)
R_{pim}[4]	9.7 (36.0)	3.2 (15.3)
Refinement		
Resolution (Å)	43.42-2.60	48.71-4.30
Reflections (working/test)	35,023/1,825	8,925/455
R_{factor}/R_{free} (%)[3]	20.1/24.3	29.4/31.1
No. of atoms (protein/ADP/water)	8,182/108/177	4,919/54/0
Model Quality		
R.m.s deviations		
Bond lengths (Å)	0.011	0.009
Bond angles (°)	1.356	1.07
Average B factor (Å^2)		
All Atoms	30.6	135.0
MinD	30.5	135.0
MinE	36.3	135.0
ADP	21.6	135.0
Water	25.3	-
Coordinate error (Å)	0.41	1.630
Ramachandran Plot		
Favored (%)	98.2	94.9
Allowed (%)	1.0	2.6

[1] Values in parenthesis are for the highest resolution shell.

[2] $R_{merge} = \Sigma_{hkl}\Sigma_i |I_i(hkl) - \langle I(hkl)\rangle| / \Sigma_{hkl}\Sigma_i I_i(hkl)$, where $I_i(hkl)$ is the intensity measured for the ith reflection and $\langle I(hkl)\rangle$ is the average intensity of all reflections with indices hkl.

[3] $R_{factor} = \Sigma_{hkl} ||F_{obs}(hkl)| - |F_{calc}(hkl)|| / \Sigma_{hkl} |F_{obs}(hkl)|$; Rfree is calculated in an identical manner using 5% of randomly selected reflections that were not included in the refinement

[4] R_{meas} = redundancy-independent (multiplicity-weighted) R_{merge}(Evans, 2006). R_{pim} = precision-indicating (multiplicity-weighted) R_{merge}(Weiss, 2001).